

Dependence of carrier mobility on grain mosaic spread in 001-oriented Si films grown on polycrystalline substrates

Woong Choi, Vladimir Matias, Jung-Kun Lee, and Alp T. Findikoglu

Citation: [Applied Physics Letters](#) **87**, 152104 (2005); doi: 10.1063/1.2103405

View online: <http://dx.doi.org/10.1063/1.2103405>

View Table of Contents: <http://scitation.aip.org/content/aip/journal/apl/87/15?ver=pdfcov>

Published by the [AIP Publishing](#)

Articles you may be interested in

[Synthesis and characterization of large-grain solid-phase crystallized polycrystalline silicon thin films](#)

J. Vac. Sci. Technol. A **32**, 061509 (2014); 10.1116/1.4897298

[Hydrogen passivation of polycrystalline silicon thin films](#)

J. Appl. Phys. **112**, 063711 (2012); 10.1063/1.4752268

[Charge transport in polycrystalline silicon thin-films on glass substrates](#)

J. Appl. Phys. **112**, 013713 (2012); 10.1063/1.4733699

[A model of electrical conduction across the grain boundaries in polycrystalline-silicon thin film transistors and metal oxide semiconductor field effect transistors](#)

J. Appl. Phys. **106**, 024504 (2009); 10.1063/1.3173179

[Electrical and structural properties of poly-Si films grown by furnace and rapid thermal annealing of amorphous Si](#)

J. Appl. Phys. **84**, 1968 (1998); 10.1063/1.368352

The advertisement features a blue background with a film strip graphic on the left. The text is in white and orange. The Oxford Instruments logo is in the bottom right corner.

Not all AFMs are created equal
Asylum Research Cypher™ AFMs
There's no other AFM like Cypher

www.AsylumResearch.com/NoOtherAFMLikeIt

OXFORD
INSTRUMENTS
The Business of Science®

Dependence of carrier mobility on grain mosaic spread in <001>-oriented Si films grown on polycrystalline substrates

Woong Choi,^{a)} Vladimir Matias, Jung-Kun Lee, and Alp T. Findikoglu^{b)}

Materials Science and Technology Division, Los Alamos National Laboratory, Los Alamos, New Mexico 87545

(Received 23 May 2005; accepted 23 August 2005; published online 4 October 2005)

We studied the dependence of carrier mobility on grain mosaic spread for <001>-oriented, 200-to-400-nm-thick Si thin films grown on polycrystalline metal substrates. The Hall mobility increased from 1% to 23% of that in bulk single-crystal Si with decreasing grain mosaic spread from 14° to 2°. For the same range of parameters, a model combining intragrain and grain boundary scattering yielded a decrease of the energy barrier height from 0.1 eV to less than 10⁻³ eV and an accompanying decrease of trap density from 6 × 10¹¹ cm⁻² to less than 3 × 10¹⁰ cm⁻². These results demonstrate that, for polycrystalline Si films, improving the intergrain alignment is an effective and practical alternative to increasing the grain size to achieve enhanced mobility. © 2005 American Institute of Physics. [DOI: 10.1063/1.2103405]

Polycrystalline Si thin films on nonsingle crystalline substrates have been of great interest for applications in thin-film transistors (TFTs) and solar cells.^{1,2} One of the critical parameters for those applications is the majority carrier mobility, which depends strongly both on the crystalline grain size and on the degree of crystalline perfection. Yet, in the research literature it is the grain size that has been primarily emphasized as the quantity that strongly influences the mobility, with little attention given to the effect of the degree of crystalline order of the grains. Recently, we reported a technique that can grow highly oriented Si thin films on polycrystalline substrates and observed that the mobility of these <001>-oriented Si films depended strongly on the grain mosaic spread, without elaborating on the physical origin of such mobility dependence.³ In this study, we expand on that experimental work and provide a plausible physical mechanism for the observed dependence of the carrier mobility on the grain mosaic spread.

To study the effects of intergrain alignment on the majority carrier transport, we prepared four series of <001>-oriented Si thin films (series A, B, C, and D). The Si films were grown on polycrystalline metal tape (Hastelloy C-276, 100 μm thick) using buffer layers composed of γ-Al₂O₃, MgO, Y₂O₃, and amorphous Al₂O₃.³ Both Si and γ-Al₂O₃ layers in each series were grown at different temperatures to create varying mosaic spread in the Si films. All the layers were deposited by electron-beam evaporation. The amorphous Al₂O₃ layer (50–75 nm) was deposited on the metal tape at room temperature as a diffusion barrier for transition metal elements. The following layers, deposited in sequence, were: a Y₂O₃ nucleation layer (5 nm) at room temperature, a biaxially oriented MgO layer (10 nm) with an assist beam of 750 eV Ar⁺ at room temperature, a homoepitaxial MgO layer (30–75 nm) at 500 °C, a γ-Al₂O₃ buffer layer (40–75 nm) at 740–800 °C, and a Si layer (200–400 nm) at 740–770 °C. For *ex situ* doping, two separate boron implants were used at 60 and at 25 keV into the Si layer that was grown with an intrinsic Si source (series A). Ion im-

planted Si samples were annealed in vacuum at 900 °C for 15 min. For *in situ* doping, the Si layer was grown with a boron-doped Si source (series B, C, and D).

The crystallographic properties of the Si layers were analyzed by x-ray diffraction (XRD). A θ -2 θ XRD scan of the multilayer indicated that the MgO, γ-Al₂O₃, and Si layers grew with (001)-orientation perpendicular to the substrate surface. For the Si (004) reflection, the full width at half maximum (FWHM) of the rocking curve $\Delta\omega_{004}$ was in the range of 1.10°–6.15° for the series. The fourfold in-plane symmetry of the Si layer was confirmed by XRD ϕ scan of the 022 reflection. The average FWHM $\Delta\phi_{022}$ was distributed between 2.20° and 12.30°. The average grain mosaic spread of each sample was analyzed using the total mosaic spread (TMS) defined as $\text{TMS} = (\Delta\omega_x^2 + \Delta\omega_y^2 + \Delta\phi_z^2)^{1/2}$, where $\Delta\omega_x$, $\Delta\omega_y$, and $\Delta\phi_z$ are tilt along *x*, tilt along *y*, and rotation along *z*, respectively.³ For the mobility measurements, the Si layer was patterned into bridge-type Hall patterns by standard photolithography and reactive ion etch. The sputtered Al (100 nm) contact electrodes were patterned by the lift-off technique, followed by annealing in forming gas (94% Ar, 6% H₂) at 350 °C for 30 min.

The carrier mobility in a thin semiconductor film (μ_f) differs from the mobility in bulk material (μ_B) if the film thickness is comparable to the carrier mean free path (λ), which depends on carrier concentration.⁴ Carrier concentrations in our Si film sets were confined to 10¹⁶–10¹⁷ cm⁻³ to minimize the variation of λ . Figure 1 shows the normalized mobility (measured Hall mobility μ_f divided by μ_B) as a function of TMS for the four series of Si films. For comparison, a commercially available 0.4-μm-thick silicon-on-sapphire (SOS) sample with a doping level of 3 × 10¹⁷ holes cm⁻³ was patterned and its mobility was measured through the same process. As is shown in Fig. 1, μ_f/μ_B of our <001>-oriented Si films shows a strong dependence on mosaic spread regardless of the doping method. Combined with single-crystal Si and SOS data, these results indicate an approximately exponential decay of mobility with TMS (dashed line). For our samples, the average in-plane grain size measured by transmission electron microscopy (TEM) was distributed between 0.3 and 0.6 μm. (TEM analyses

^{a)}Electronic mail: woong@lanl.gov

^{b)}Electronic mail: findik@lanl.gov

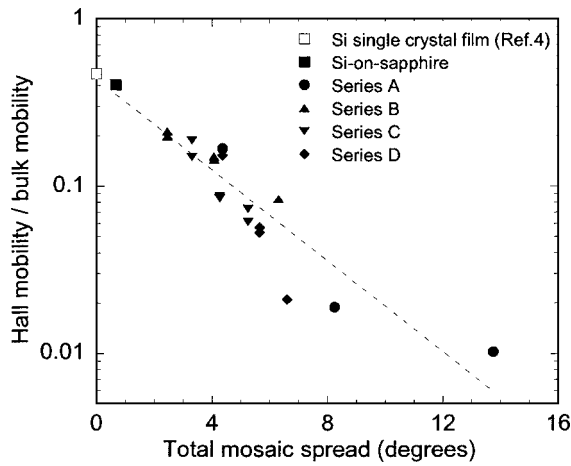


FIG. 1. Normalized Hall mobility (μ_f/μ_B) as a function of total mosaic spread. Mobility of silicon-on-sapphire was measured through the same process for comparison. The mobility of a single crystal Si thin film was estimated according to Ref. 4. Dashed line is a guide for the eye.

were included in our earlier publication.³) Since mobility can be regarded to vary linearly with the grain size in this range,⁵ the factor of 20 change in μ_f/μ_B cannot be dominated by the changes in the grain size. Also, the root mean square surface roughness measured by atomic force microscopy was scattered in the range of 11–28 nm on a $5 \times 5 \mu\text{m}^2$ scale, revealing no significant correlation with μ_f/μ_B . Therefore, we conclude that in our study the effects of grain size and surface roughness were negligible for the observed μ_f/μ_B dependence on TMS.

The effective mobility (μ_{eff}) in polycrystalline Si can be described by combining the mobility in the grain (μ_G) and at the grain boundary (μ_{GB})⁶

$$\mu_{\text{eff}}^{-1} = \mu_G^{-1} + \mu_{\text{GB}}^{-1}, \quad (1)$$

where $\mu_G = C\mu_B$ (C : constant) (Ref. 7) and $\mu_{\text{GB}} = C'qL(2\pi m^*kT)^{-1/2}e^{-E_B/kT}$ (C' : constant, q : unit charge, L : grain size, m^* : effective mass, k : Boltzmann constant, T : temperature, and E_B : energy barrier height at the grain boundary).^{6,8} Figure 2 shows the measured Hall mobility versus inverse temperature for four Si thin films with varying

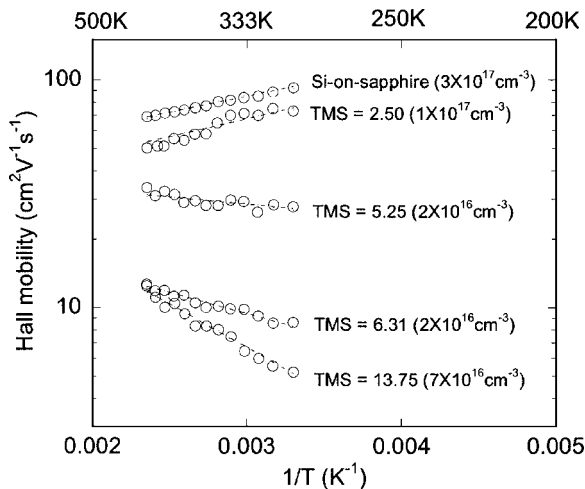


FIG. 2. Hall mobility as a function of inverse temperature for Si films with different values of grain total mosaic spread along with the silicon-on-sapphire. Shown in parenthesis are the carrier concentrations of the samples. Dashed lines are curve fits based on Eq. (1).

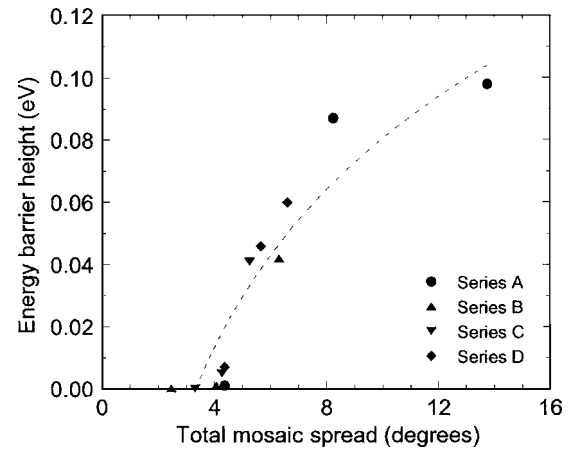


FIG. 3. Energy barrier height at grain boundaries (E_B) as a function of total mosaic spread, estimated based on Eq. (1). Dashed line is a guide for the eye.

TMS along with that of the SOS. The dashed lines are curve fits using Eq. (1), with μ_B based on the expression by Arora *et al.*⁹ In the modeling, C' and E_B are fit parameters while C , extrapolated from data in Fig. 1 for zero mosaic spread, is fixed at 0.47. For these samples, C' was in the range of 0–0.05 and was weakly correlated with the mosaic spread, whereas the energy barrier E_B increased monotonically with the mosaic spread (Fig. 3). In Fig. 2, the mobility of the SOS sample decreases as the temperature is raised, exhibiting the dominant effect of intragrain scattering. For Si films with TMS less than 5° , the mobility behaves similarly to that of the SOS with negligible contribution of grain boundary scattering ($E_B \leq 10^{-3}$ eV). Our current model and measurements cannot resolve E_B less than about 1 meV. However, both the model and measurements allow us to distinguish a transition from intergrain scattering dominated mobility to intragrain scattering dominated mobility with decreasing TMS. It is possible that the mobility of these well-oriented Si films may reach that of the SOS if an improved process could reduce the surface roughness and the level of defects to be comparable to those of the SOS. On the other hand, for Si films with TMS $\sim 5^\circ$, the mobilities barely increase with temperature, suggesting comparable contribution of intragrain and grain boundary scattering. As the TMS increases further up to 13.75° , the mobilities increase with larger slopes, indicating the dominant contribution of grain boundary scattering. Earlier work has shown that, in polycrystalline Si films with grains of several microns in size, the carrier transport is dominated by intragrain scattering.¹⁰ Our results indicate that enhancing intergrain alignment while keeping the grains small produces effectively the same result that enlarging grain size does. Thus, using well-aligned buffer layers to achieve improved mobility could be considered as an alternative fabrication method in TFT and solar cell applications, where laser annealing or other techniques are typically used to increase the grain size, and thereby the mobility.

If depletion within the grain is negligible, E_B can be related to the trap density at the grain boundary Q_t , as⁸

$$E_B = qQ_t^2/8\epsilon_0\epsilon_{\text{Si}}N, \quad (2)$$

where ϵ_0 is the permittivity of vacuum, ϵ_{Si} is the dielectric constant of Si, and N is the carrier concentration. Trap densities calculated using Eq. (2) are shown with respect to TMS in Fig. 4, where trap density increases from less than 3

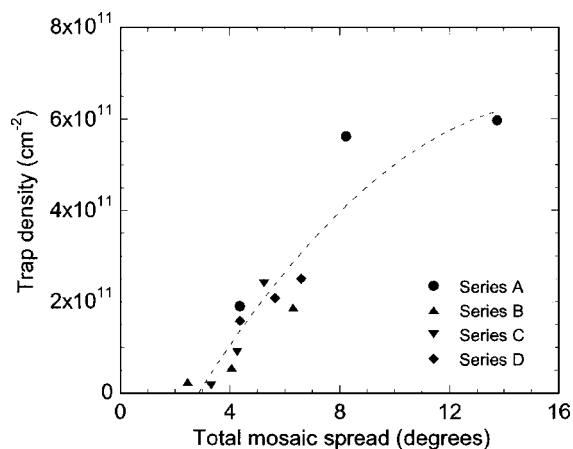


FIG. 4. Trap density at grain boundaries as a function of total mosaic spread, calculated using Eq. (2). Dashed line is a guide for the eye.

$\times 10^{10} \text{ cm}^{-2}$ to $6 \times 10^{11} \text{ cm}^{-2}$ with increasing TMS. One possible source for the trapping states is dislocations at grain boundaries since it has been reported that the dislocation density increases with misorientation up to 16° .¹¹ Another possible source is impurity segregation at grain boundaries: The degree of segregation may be determined by the grain boundary energy, and this is known to increase with misorientation up to 15° .¹² Regardless of the nature of the trapping states, the trap density is expected to increase with grain mosaic spread. Within the scope of our present study, it is difficult to determine with certainty the relative importance of the aforementioned mechanisms.

In conclusion, we have studied the relationship between mobility and grain mosaic spread for $\langle 001 \rangle$ -oriented Si thin films grown on polycrystalline substrates. The Hall mobility increased from 1% to 23% of that in bulk single-crystal Si as

the grain mosaic spread decreased from 14° to 2° . Based on a model combining the intragrain and grain boundary mobility, we calculated the energy barrier at grain boundaries, which decreased from 0.1 eV to less than 10^{-3} eV with decreasing grain mosaic spread. The estimated trap density at the grain boundaries also decreased from $6 \times 10^{11} \text{ cm}^{-2}$ to less than $3 \times 10^{10} \text{ cm}^{-2}$ with decreasing grain mosaic spread. These results indicate that improved grain alignment leads to significantly enhanced majority carrier mobility in polycrystalline Si films, with potentially important implications for TFT and solar cell applications.

This work was funded from Laboratory Directed Research and Development—Exploratory Research (20030355ER) at Los Alamos National Laboratory. The authors thank Jeffrey O. Willis for his useful comments on the manuscript.

¹S. D. Brotherton, *Semicond. Sci. Technol.* **10**, 721 (1995).

²A. Shah, P. Torres, R. Tschamer, N. Wyrsh, and H. Keppner, *Science* **285**, 692 (1999).

³A. T. Findikoglu, W. Choi, V. Matias, T. G. Holesinger, Q. X. Jia, and D. E. Peterson, *Adv. Mater. (Weinheim, Ger.)* **17**, 1527 (2005).

⁴H. F. Wolf, *Semiconductors* (Wiley, New York, 1971), pp. 274–289.

⁵J. Martinez and J. Piqueras, *Solid-State Electron.* **23**, 297 (1980).

⁶J. Levinson, F. R. Shepherd, P. J. Scanlon, W. D. Westwood, G. Estes, and M. Rider, *J. Appl. Phys.* **53**, 1193 (1982).

⁷L. L. Kazmerski, W. B. Berry, and C. W. Allen, *J. Appl. Phys.* **43**, 3515 (1972).

⁸J. Y. W. Seto, *J. Appl. Phys.* **46**, 5247 (1975).

⁹N. D. Arora, J. R. Hauser, and D. J. Roulston, *IEEE Trans. Electron Devices* **ED-29**, 292 (1982).

¹⁰Y. Morimoto, Y. Jinno, K. Hirai, H. Ogata, T. Yamada, and K. Yoneda, *J. Electrochem. Soc.* **144**, 2495 (1997).

¹¹C. R. M. Grovenor, *J. Phys. C* **18**, 4079 (1985).

¹²C. S. Nichols, R. F. Cook, D. R. Clarke, and D. A. Smith, *Acta Metall. Mater.* **39**, 1657 (1991).